15. QUARK MODEL

Revised August 2015 by C. Amsler (University of Bern), T. DeGrand (University of Colorado, Boulder), and B. Krusche (University of Basel).

15.1. Quantum numbers of the quarks

Quantum chromodynamics (QCD) is the theory of the strong interactions. QCD is a quantum field theory and its constituents are a set of fermions, the quarks, and gauge bosons, the gluons. Strongly interacting particles, the hadrons, are bound states of quark and gluon fields. As gluons carry no intrinsic quantum numbers beyond color charge, and because color is believed to be permanently confined, most of the quantum numbers of strongly interacting particles are given by the quantum numbers of their constituent quarks and antiquarks. The description of hadronic properties which strongly emphasizes the role of the minimum-quark-content part of the wave function of a hadron is generically called the quark model. It exists on many levels: from the simple, almost dynamics-free picture of strongly interacting particles as bound states of quarks and antiquarks, to more detailed descriptions of dynamics, either through models or directly from QCD itself. The different sections of this review survey the many approaches to the spectroscopy of strongly interacting particles which fall under the umbrella of the quark model.

Table 15.1: Additive quantum numbers of the quarks.

	d	u	s	c	b	t
Q – electric charge	$-\frac{1}{3}$	$+\frac{2}{3}$	$-\frac{1}{3}$	$+\frac{2}{3}$	$-\frac{1}{3}$	$+\frac{2}{3}$
I – isospin	$\frac{1}{2}$	$\frac{1}{2}$	0	0	0	0
I_z – isospin z-component	$-\frac{1}{2}$	$+\frac{1}{2}$	0	0	0	0
S – strangeness	0	0	-1	0	0	0
C – charm	0	0	0	$+1$	0	0
B – bottomness	0	0	0	0	-1	0
T – topness	0	0	0	0	0	$+1$

Quarks are strongly interacting fermions with spin 1/2 and, by convention, positive parity. Antiquarks have negative parity. Quarks have the additive baryon number 1/3, antiquarks -1/3. Table 15.1 gives the other additive quantum numbers (flavors) for the three generations of quarks. They are related to the charge Q (in units of the elementary charge e) through the generalized Gell-Mann-Nishijima formula

$$\mathsf{Q} = \mathsf{I}_z + \frac{\mathcal{B} + \mathsf{S} + \mathsf{C} + \mathsf{B} + \mathsf{T}}{2} \ , \tag{15.1}$$

where $\mathcal{B}$ is the baryon number. The convention is that the *flavor* of a quark (I_z, S, C, B, or T) has the same sign as its *charge* Q. With this convention, any flavor carried by a charged meson has the same sign as its charge, *e.g.*, the strangeness of the K^+ is $+1$, the bottomness of the B^+ is $+1$, and the charm and strangeness of the D_s^- are each -1. Antiquarks have the opposite flavor signs. The hypercharge is defined as

$$\mathsf{Y} = \mathcal{B} + \mathsf{S} - \frac{\mathsf{C} - \mathsf{B} + \mathsf{T}}{3} \ .$$

Thus Y is equal to $\frac{1}{3}$ for the u and d quarks, $-\frac{2}{3}$ for the s quark, and 0 for all other quarks.

15.2. Mesons

Mesons have baryon number $\mathcal{B} = 0$. In the quark model, they are $q\overline{q}'$ bound states of quarks q and antiquarks $\overline{q}'$ (the flavors of q and q' may be different). If the orbital angular momentum of the $q\overline{q}'$ state is ℓ, then the parity P is $(-1)^{\ell+1}$. The meson spin J is given by the usual relation $|\ell - s| \leq J \leq |\ell + s|$, where s is 0 (antiparallel quark spins) or 1 (parallel quark spins). The charge conjugation, or C-parity $C = (-1)^{\ell+s}$, is defined only for the $q\bar{q}$ states made of quarks and their own antiquarks. The C-parity can be generalized to the G-parity $G = (-1)^{I+\ell+s}$ for mesons made of quarks and their own antiquarks (isospin $\mathsf{I}_z = 0$), and for the charged $u\bar{d}$ and $d\bar{u}$ states (isospin $\mathsf{I} = 1$).

The mesons are classified in J^{PC} multiplets. The $\ell = 0$ states are the pseudoscalars (0^{-+}) and the vectors (1^{--}). The orbital excitations $\ell = 1$ are the scalars (0^{++}), the axial vectors (1^{++}) and (1^{+-}), and the tensors (2^{++}). Assignments for many of the known mesons are given in Tables 15.2 and 15.3. Radial excitations are denoted by the principal quantum number n. The very short lifetime of the t quark makes it likely that bound-state hadrons containing t quarks and/or antiquarks do not exist.

States in the natural spin-parity series $P = (-1)^J$ must, according to the above, have $s = 1$ and hence, $CP = +1$. Thus, mesons with natural spin-parity and $CP = -1$ (0^{+-}, 1^{-+}, 2^{+-}, 3^{-+}, *etc.*) are forbidden in the $q\bar{q}'$ model. The $J^{PC} = 0^{--}$ state is forbidden as well. Mesons with such *exotic* quantum numbers may exist, but would lie outside the $q\bar{q}'$ model (see section below on exotic mesons).

Following SU(3), the nine possible $q\bar{q}'$ combinations containing the light u, d, and s quarks are grouped into an octet and a singlet of light quark mesons:

$$\mathbf{3} \otimes \overline{\mathbf{3}} = \mathbf{8} \oplus \mathbf{1} \ . \tag{15.2}$$

A fourth quark such as charm c can be included by extending SU(3) to SU(4). However, SU(4) is badly broken owing to the much heavier c quark. Nevertheless, in an SU(4) classification, the sixteen mesons are grouped into a 15-plet and a singlet:

$$\mathbf{4} \otimes \overline{\mathbf{4}} = \mathbf{15} \oplus \mathbf{1} \ . \tag{15.3}$$

Table 15.2: Suggested $q\overline{q}$ quark-model assignments for some of the observed light mesons. Mesons in bold face are included in the Meson Summary Table. The wave functions f and f' are given in the text. The singlet-octet mixing angles from the quadratic and linear mass formulae are also given for the well established nonets. The classification of the 0^{++} mesons is tentative: the light scalars $a_0(980)$, $f_0(980)$, $f_0(500)$ and $K_0^*(800)$ are often considered to be meson-meson resonances or four-quark states, and are omitted from the table. The isoscalar 0^{++} mesons are expected to mix. In particular, the $f_0(1710)$ mixes with the $f_0(1500)$ and the $f_0(1370)$. The $a_0(1450)$ is not firmly established. See the "Note on Non-$q\overline{q}$ mesons" and the "Note on Scalar Mesons" in the Meson Listings for details and alternative schemes. In the 1^{++} nonet the isoscalar slot is disputed by the $f_1(1510)$. The isoscalar assignments in the 2^1S_0 (0^{++}) nonet are also tentative. See the "Note on The Pseudoscalar and Pseudovector Mesons in the 1400 MeV Region" in the Meson Listings.

$n\,^{2s+1}\ell_J$	J^{PC}	$\mathsf{I}=1$ $u\overline{d}$, $\overline{u}d$, $\frac{1}{\sqrt{2}}(d\overline{d}-u\overline{u})$	$\mathsf{I}=\frac{1}{2}$ $u\overline{s}$, $d\overline{s}$; $\overline{d}s$, $-\overline{u}s$	$\mathsf{I}=0$ f'	$\mathsf{I}=0$ f	$\theta_{\rm quad}$ [°]	$\theta_{\rm lin}$ [°]
$1\,^1S_0$	0^{-+}	$\boldsymbol{\pi}$	$\boldsymbol{K}$	$\boldsymbol{\eta}$	$\boldsymbol{\eta'(958)}$	-11.4	-24.5
$1\,^3S_1$	1^{--}	$\boldsymbol{\rho(770)}$	$\boldsymbol{K^*(892)}$	$\boldsymbol{\phi(1020)}$	$\boldsymbol{\omega(782)}$	39.1	36.4
$1\,^1P_1$	1^{+-}	$\boldsymbol{b_1(1235)}$	$\boldsymbol{K_{1B}}^\dagger$	$h_1(1380)$	$\boldsymbol{h_1(1170)}$		
$1\,^3P_0$	0^{++}	$\boldsymbol{a_0(1450)}$	$\boldsymbol{K_0^*(1430)}$	$\boldsymbol{f_0(1710)}$	$\boldsymbol{f_0(1370)}$		
$1\,^3P_1$	1^{++}	$\boldsymbol{a_1(1260)}$	$\boldsymbol{K_{1A}}^\dagger$	$\boldsymbol{f_1(1420)}$	$\boldsymbol{f_1(1285)}$		
$1\,^3P_2$	2^{++}	$\boldsymbol{a_2(1320)}$	$\boldsymbol{K_2^*(1430)}$	$\boldsymbol{f_2'(1525)}$	$\boldsymbol{f_2(1270)}$	32.1	30.5
$1\,^1D_2$	2^{-+}	$\boldsymbol{\pi_2(1670)}$	$\boldsymbol{K_2(1770)}^\dagger$	$\eta_2(1870)$	$\boldsymbol{\eta_2(1645)}$		
$1\,^3D_1$	1^{--}	$\boldsymbol{\rho(1700)}$	$\boldsymbol{K^*(1680)}$		$\boldsymbol{\omega(1650)}$		
$1\,^3D_2$	2^{--}		$\boldsymbol{K_2(1820)}$				
$1\,^3D_3$	3^{--}	$\boldsymbol{\rho_3(1690)}$	$\boldsymbol{K_3^*(1780)}$	$\boldsymbol{\phi_3(1850)}$	$\boldsymbol{\omega_3(1670)}$	31.8	30.8
$1\,^3F_4$	4^{++}	$\boldsymbol{a_4(2040)}$	$\boldsymbol{K_4^*(2045)}$		$\boldsymbol{f_4(2050)}$		
$1\,^3G_5$	5^{--}	$\rho_5(2350)$	$K_5^*(2380)$				
$1\,^3H_6$	6^{++}	$a_6(2450)$			$f_6(2510)$		
$2\,^1S_0$	0^{-+}	$\boldsymbol{\pi(1300)}$	$K(1460)$	$\boldsymbol{\eta(1475)}$	$\boldsymbol{\eta(1295)}$		
$2\,^3S_1$	1^{--}	$\boldsymbol{\rho(1450)}$	$\boldsymbol{K^*(1410)}$	$\boldsymbol{\phi(1680)}$	$\boldsymbol{\omega(1420)}$		

† The $1^{+\pm}$ and $2^{-\pm}$ isospin $\frac{1}{2}$ states mix. In particular, the K_{1A} and K_{1B} are nearly equal (45°) mixtures of the $K_1(1270)$ and $K_1(1400)$. The physical vector mesons listed under 1^3D_1 and 2^3S_1 may be mixtures of 1^3D_1 and 2^3S_1.

Table 15.3: $q\overline{q}$ quark-model assignments for the observed heavy mesons with established J^{PC}. Mesons in bold face are included in the Meson Summary Table.

$n\,^{2s+1}\ell_J$	J^{PC}	I = 0 $c\overline{c}$	I = 0 $b\overline{b}$	I = $\frac{1}{2}$ $c\overline{u}$, $c\overline{d}$; $\overline{c}u$, $\overline{c}d$	I = 0 $c\overline{s}$; $\overline{c}s$	I = $\frac{1}{2}$ $b\overline{u}$, $b\overline{d}$; $\overline{b}u$, $\overline{b}d$	I = 0 $b\overline{s}$; $\overline{b}s$	I = 0 $b\overline{c}$; $\overline{b}c$
$1\,^1S_0$	0^{-+}	$\boldsymbol{\eta_c(1S)}$	$\boldsymbol{\eta_b(1S)}$	$\boldsymbol{D}$	$\boldsymbol{D_s^{\pm}}$	$\boldsymbol{B}$	$\boldsymbol{B_s^0}$	$\boldsymbol{B_c^{\pm}}$
$1\,^3S_1$	1^{--}	$\boldsymbol{J/\psi(1S)}$	$\boldsymbol{\Upsilon(1S)}$	$\boldsymbol{D^*}$	$\boldsymbol{D_s^{*\pm}}$	$\boldsymbol{B^*}$	B_s^*	
$1\,^1P_1$	1^{+-}	$\boldsymbol{h_c(1P)}$	$\boldsymbol{h_b(1P)}$	$\boldsymbol{D_1(2420)}$	$\boldsymbol{D_{s1}(2536)^{\pm}}$	$\boldsymbol{B_1(5721)}$	$\boldsymbol{B_{s1}(5830)^0}$	
$1\,^3P_0$	0^{++}	$\boldsymbol{\chi_{c0}(1P)}$	$\boldsymbol{\chi_{b0}(1P)}$	$\boldsymbol{D_0^*(2400)}$	$\boldsymbol{D_{s0}^*(2317)^{\pm\dagger}}$			
$1\,^3P_1$	1^{++}	$\boldsymbol{\chi_{c1}(1P)}$	$\boldsymbol{\chi_{b1}(1P)}$	$D_1(2430)$	$\boldsymbol{D_{s1}(2460)^{\pm\dagger}}$			
$1\,^3P_2$	2^{++}	$\boldsymbol{\chi_{c2}(1P)}$	$\boldsymbol{\chi_{b2}(1P)}$	$\boldsymbol{D_2^*(2460)}$	$\boldsymbol{D_{s2}^*(2573)^{\pm}}$	$\boldsymbol{B_2^*(5747)}$	$\boldsymbol{B_{s2}^*(5840)^0}$	
$1\,^3D_1$	1^{--}	$\boldsymbol{\psi(3770)}$			$D_{s1}^*(2860)^{\pm\ddagger}$			
$1\,^3D_3$	3^{--}				$D_{s3}^*(2860)^{\pm}$			
$2\,^1S_0$	0^{-+}	$\boldsymbol{\eta_c(2S)}$	$\eta_b(2S)$	$D(2550)$				
$2\,^3S_1$	1^{--}	$\boldsymbol{\psi(2S)}$	$\boldsymbol{\Upsilon(2S)}$		$\boldsymbol{D_{s1}^*(2700)^{\pm\ddagger}}$			
$2\,^1P_1$	1^{+-}		$h_b(2P)$					
$2\,^3P_{0,1,2}$	$0^{++}, 1^{++}, 2^{++}$	$\boldsymbol{\chi_{c0,2}(2P)}$	$\boldsymbol{\chi_{b0,1,2}(2P)}$					
$3\,^3P_{0,1,2}$	$0^{++}, 1^{++}, 2^{++}$		$\boldsymbol{\chi_b(3P)}$					

† The masses of these states are considerably smaller than most theoretical predictions. They have also been considered as four-quark states.

‡ These states are mixtures of the $1\,^3D_1$ and $2\,^3S_1$ states.

The open flavor states in the 1^{+-} and 1^{++} rows are mixtures of the $1^{+\pm}$ states.

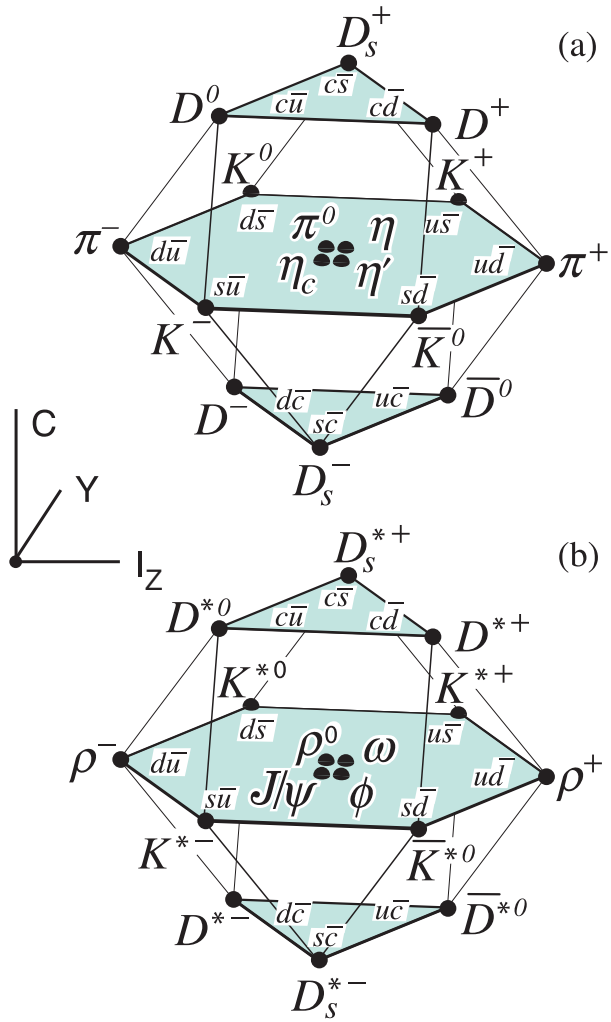

Figure 15.1: SU(4) weight diagram showing the 16-plets for the pseudoscalar (a) and vector mesons (b) made of the u, d, s, and c quarks as a function of isospin I_z, charm C, and hypercharge $\mathsf{Y} = \mathcal{B} + \mathsf{S} - \frac{\mathsf{C}}{3}$. The nonets of light mesons occupy the central planes to which the $c\bar{c}$ states have been added.

The *weight diagrams* for the ground-state pseudoscalar (0^{-+}) and vector (1^{--}) mesons are depicted in Fig. 15.1. The light quark mesons are members of nonets building the middle plane in Fig. 15.1(a) and (b).

Isoscalar states with the same J^{PC} will mix, but mixing between the two light quark isoscalar mesons, and the much heavier charmonium or bottomonium states, are generally assumed to be negligible. In the following, we shall use the generic names a for the $\mathsf{I} = 1$, K for the $\mathsf{I} = 1/2$, and f and f' for the $\mathsf{I} = 0$ members of the light quark nonets. Thus, the physical isoscalars are mixtures of the SU(3) wave function ψ_8 and ψ_1:

$$f' = \psi_8 \cos\theta - \psi_1 \sin\theta \ , \tag{15.4}$$

$$f = \psi_8 \sin\theta + \psi_1 \cos\theta \ , \tag{15.5}$$

where θ is the nonet mixing angle and

$$\psi_8 = \frac{1}{\sqrt{6}}(u\bar{u} + d\bar{d} - 2s\bar{s}) \ , \tag{15.6}$$

$$\psi_1 = \frac{1}{\sqrt{3}}(u\bar{u} + d\bar{d} + s\bar{s}) \ . \tag{15.7}$$

These mixing relations are often rewritten to exhibit the $u\bar{u} + d\bar{d}$ and $s\bar{s}$ components which decouple for the "ideal" mixing angle θ_i, such that $\tan\,\theta_i = 1/\sqrt{2}$ (or $\theta_i = 35.3°$). Defining $\alpha = \theta + 54.7°$, one obtains the physical isoscalar in the flavor basis

$$f' = \frac{1}{\sqrt{2}}(u\bar{u} + d\bar{d})\cos\alpha - s\bar{s}\ \sin\alpha \ , \tag{15.8}$$

and its orthogonal partner f (replace α by α –90°). Thus for ideal mixing ($\alpha_i = 90°$), the f' becomes pure $s\bar{s}$ and the f pure $u\bar{u} + d\bar{d}$. The mixing angle θ can be derived by diagonalizing the mass matrix

$$\begin{pmatrix} m_8 & m_{81} \\ m_{18} & m_1 \end{pmatrix}$$

The mass eigenvalues are $m_{f'}$ and m_f. The mixing angle is given by

$$\tan\theta = \frac{m_8 - m_{f'}}{m_{81}} \ .$$

Calculating m_8 and m_{81} from the wave functions Eq. (15.6) and Eq. (15.7), and expressing the quark masses as a function of the $\mathsf{I} = 1/2$ and $\mathsf{I} = 1$ meson masses, one obtains

$$\tan\theta = \frac{4m_K - m_a - 3m_{f'}}{2\sqrt{2}(m_a - m_K)} \ , \tag{15.9}$$

which also determines the sign of θ. Alternatively, one can express the mixing angle as a function of all nonet masses. The octet mass is given by

$$m_8 = m_{f'}\cos^2\theta + m_f\sin^2\theta$$

whence

$$\tan^2\theta = \frac{4m_K - m_a - 3m_{f'}}{-4m_K + m_a + 3m_f} \ . \tag{15.10}$$

Eliminating θ from Eq. (15.9) and Eq. (15.10) leads to the sum rule [1]

$$(m_f + m_{f'})(4m_K - m_a) - 3m_f m_{f'} = 8m_K^2 - 8m_K m_a + 3m_a^2. \tag{15.11}$$

This relation is verified for the ground-state vector mesons. We identify the $\phi(1020)$ with the f' and the $\omega(783)$ with the f. Thus

$$\phi(1020) = \psi_8\ \cos\theta_V - \psi_1\ \sin\theta_V \ , \tag{15.12}$$

$$\omega(782) = \psi_8 \sin\theta_V + \psi_1 \cos\theta_V \ , \tag{15.13}$$

with the vector mixing angle $\theta_V = 36.4°$ from Eq. (15.10), very close to ideal mixing. Thus $\phi(1020)$ is nearly pure $s\bar{s}$. For ideal mixing, Eq. (15.9) and Eq. (15.10) lead to the relations

$$m_K = \frac{m_f + m_{f'}}{2} \ , \quad m_a = m_f \ , \tag{15.14}$$

which are satisfied for the vector mesons.

The situation for the pseudoscalar and scalar mesons is not so clear cut, either theoretically or experimentally. For the pseudoscalars, the mixing angle is small. This can be understood qualitatively via gluon-line counting of the mixing process. The size of the mixing process between the nonstrange and strange mass bases scales as α_s^2, not α_s^3, because of two rather than three gluon exchange as it does for the vector mesons. It may also be that the lightest isoscalar pseudoscalars mix more strongly with excited states or with states of substantial non-$\bar{q}q$ content, as will be discussed below.

A variety of analysis methods lead to similar results: First, for these states, Eq. (15.11) is satisfied only approximately. Then Eq. (15.9) and Eq. (15.10) lead to somewhat different values for the mixing angle. Identifying the η with the f' one gets

$$\eta = \psi_8 \cos\theta_P - \psi_1 \sin\theta_P \ , \tag{15.15}$$

$$\eta' = \psi_8 \sin\theta_P + \psi_1 \cos\theta_P \ . \tag{15.16}$$

Following chiral perturbation theory, the meson masses in the mass formulae (Eq. (15.9) and Eq. (15.10)) might be replaced by their squares. Table 15.2 lists the mixing angle $\theta_{\rm lin}$ from Eq. (15.10) (using the neutral members of the nonets) and the corresponding $\theta_{\rm quad}$ obtained by replacing the meson masses by their squares throughout.

The pseudoscalar mixing angle θ_P can also be measured by comparing the partial widths for radiative J/ψ decay into a vector and a pseudoscalar [2], radiative $\phi(1020)$ decay into η and η' [3], or $\bar{p}p$ annihilation at rest into a pair of vector and pseudoscalar or into two pseudoscalars [4,5]. One obtains a mixing angle between –10° and –20°. More recently, a lattice QCD simulation, Ref. 6, has successfully reproduced the masses of the η and η', and as a byproduct find a mixing angle $\theta_{lin} = -14.1(2.8)°$. We return to this point in Sec. 15.6.

The nonet mixing angles can be measured in $\gamma\gamma$ collisions, *e.g.*, for the 0^{-+}, 0^{++}, and 2^{++} nonets. In the quark model, the amplitude for the coupling of neutral mesons to two photons is proportional to $\sum_i Q_i^2$, where Q_i is the charge of the i-th quark. The 2γ partial width of an isoscalar meson with mass m is then given in terms of the mixing angle α by

$$\Gamma_{2\gamma} = C(5\cos\alpha - \sqrt{2}\sin\alpha)^2 m^3 \ , \tag{15.17}$$

for f' and f ($\alpha \to \alpha - 90°$). The coupling C may depend on the meson mass. It is often assumed to be a constant in the nonet. For the isovector a, one then finds $\Gamma_{2\gamma} = 9\ C\ m^3$. Thus the members of an ideally mixed nonet couple to 2γ with partial widths in the ratios

$f : f' : a = 25 : 2 : 9$. For tensor mesons, one finds from the ratios of the measured 2γ partial widths for the $f_2(1270)$ and $f_2'(1525)$ mesons a mixing angle α_T of $(81\pm 1)^\circ$, or $\theta_T = (27 \pm 1)^\circ$, in accord with the linear mass formula. For the pseudoscalars, one finds from the ratios of partial widths $\Gamma(\eta' \to 2\gamma)/\Gamma(\eta \to 2\gamma)$ a mixing angle $\theta_P = (-18 \pm 2)^\circ$, while the ratio $\Gamma(\eta' \to 2\gamma)/\Gamma(\pi^0 \to 2\gamma)$ leads to $\sim -24\ ^\circ$. SU(3) breaking effects for pseudoscalars are discussed in Ref. 7.

The partial width for the decay of a scalar or a tensor meson into a pair of pseudoscalar mesons is model-dependent. Following Ref. 8,

$$\Gamma = C \times \gamma^2 \times |F(q)|^2 \times q \ . \tag{15.18}$$

C is a nonet constant, q the momentum of the decay products, $F(q)$ a form factor, and γ^2 the SU(3) coupling. The model-dependent form factor may be written as

$$|F(q)|^2 = q^{2\ell} \times \exp(-\frac{q^2}{8\beta^2}), \tag{15.19}$$

where ℓ is the relative angular momentum between the decay products. The decay of a $q\bar{q}$ meson into a pair of mesons involves the creation of a $q\bar{q}$ pair from the vacuum, and SU(3) symmetry assumes that the matrix elements for the creation of $s\bar{s}$, $u\bar{u}$, and $d\bar{d}$ pairs are equal. The couplings γ^2 are given in Table 15.4, and their dependence upon the mixing angle α is shown in Fig. 15.2 for isoscalar decays. The generalization to unequal $s\bar{s}$, $u\bar{u}$, and $d\bar{d}$ couplings is given in Ref. 8. An excellent fit to the tensor meson decay widths is obtained assuming SU(3) symmetry, with $\beta \simeq 0.5$ GeV/c, $\theta_V \simeq 26\ ^\circ$ and $\theta_P \simeq -17\ ^\circ$ [8].

15.3. Exotic mesons

The existence of a light nonet composed of four quarks with masses below 1 GeV was suggested a long time ago [9]. Coupling two triplets of light quarks u, d, and s, one obtains nine states, of which the six symmetric ($uu,\ dd,\ ss,\ ud+du,\ us+su,\ ds+sd$) form the six dimensional representation **6**, while the three antisymmetric ($ud-du,\ us-su,\ ds-sd$) form the three dimensional representation $\overline{\mathbf{3}}$ of SU(3):

$$\mathbf{3} \otimes \mathbf{3} = \mathbf{6} \oplus \overline{\mathbf{3}} \ . \tag{15.20}$$

Combining with spin and color and requiring antisymmetry, one finds that the most deeply bound diquark (and hence the lightest) is the one in the $\overline{\mathbf{3}}$ and spin singlet state. The combination of the diquark with an antidiquark in the **3** representation then gives a light nonet of four-quark scalar states. Letting the number of strange quarks determine the mass splitting, one obtains a mass inverted spectrum with a light isosinglet ($ud\bar{u}\bar{d}$), a medium heavy isodoublet (*e.g.*, $ud\bar{s}\bar{d}$) and a heavy isotriplet (*e.g.*, $ds\bar{u}\bar{s}$) + isosinglet (*e.g.*, $us\bar{u}\bar{s}$). It is then tempting to identify the lightest state with the $f_0(500)$, and the heaviest states with the $a_0(980)$, and $f_0(980)$. Then the meson with strangeness $K_0^*(800)$ would lie in-between.

Table 15.4: SU(3) couplings γ^2 for quarkonium decays as a function of nonet mixing angle α, up to a common multiplicative factor C ($\phi \equiv 54.7^\circ + \theta_P$).

Isospin	Decay channel	γ^2
0	$\pi\pi$	$3\cos^2\alpha$
	$K\overline{K}$	$(\cos\alpha - \sqrt{2}\sin\alpha)^2$
	$\eta\eta$	$(\cos\alpha\cos^2\phi - \sqrt{2}\sin\alpha\sin^2\phi)^2$
	$\eta\eta'$	$\frac{1}{2}\sin^2 2\phi\ (\cos\alpha + \sqrt{2}\sin\alpha)^2$
1	$\eta\pi$	$2\ \cos^2\phi$
	$\eta'\pi$	$2\ \sin^2\phi$
	$K\overline{K}$	1
$\frac{1}{2}$	$K\pi$	$\frac{3}{2}$
	$K\eta$	$(\sin\phi - \frac{\cos\phi}{\sqrt{2}})^2$
	$K\eta'$	$(\cos\phi + \frac{\sin\phi}{\sqrt{2}})^2$

QCD predicts the existence of extra isoscalar mesons. In the pure gauge theory they contain only gluons, and are called the glueballs. The ground state glueball is predicted by lattice gauge theories to be 0^{++}, the first excited state 2^{++}. Errors on the mass predictions are large. From Ref. 10 one obtains 1750 (50) (80) MeV for the mass of the lightest 0^{++} glueball from quenched QCD. As an example for the glueball mass spectrum, we show in Fig. 15.3 a calculation from Ref. 11. A mass of 1710 MeV is predicted for the ground state, also with an error of about 100 MeV. Earlier work by other groups produced masses at 1650 MeV [12] and 1550 MeV [13] (see also [14]). The first excited state has a mass of about 2.4 GeV, and the lightest glueball with exotic quantum numbers (2^{+-}) has a mass of about 4 GeV.

These calculations are made in the so-called "quenched approximation" which neglects $q\bar{q}$ loops. However, both glue and $q\bar{q}$ states will couple to singlet scalar mesons. Therefore glueballs will mix with nearby $q\bar{q}$ states of the same quantum numbers. For example, the two isoscalar 0^{++} mesons around 1500 MeV will mix with the pure ground state glueball to generate the observed physical states $f_0(1370)$, $f_0(1500)$, and $f_0(1710)$ [8,15]. The first results from lattice calculations, which include these effects, indicate that the mass shifts are small. We return to a discussion of this point in Sec. 15.6.

The existence of three singlet scalar mesons around 1.5 GeV suggests additional degrees of freedom such as glue, since only two mesons are predicted in this mass range. The $f_0(1500)$ [8,15] or, alternatively, the $f_0(1710)$ [12], have been proposed as candidates for the scalar glueball, both states having considerable mixing also with the $f_0(1370)$.

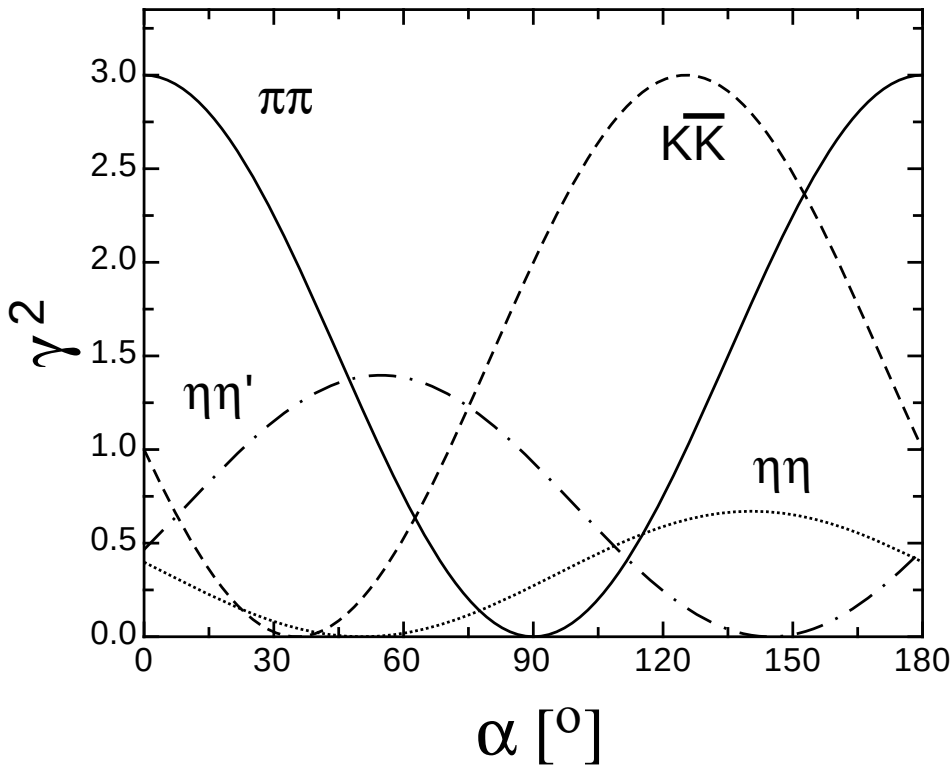

Figure 15.2: SU(3) couplings as a function of mixing angle α for isoscalar decays, up to a common multiplicative factor C and for $\theta_P = -17.3°$.

Other mixing schemes, in particular with the $f_0(500)$ and the $f_0(980)$, have also been proposed [16]. Details can be found in the "Note on Non-$q\bar{q}$ Mesons" in the Meson Listings and in Ref. 17 See also the "Note on Scalar Mesons below 2 GeV".

Mesons made of $q\bar{q}$ pairs bound by excited gluons g, the hybrid states $q\bar{q}g$, are also predicted. They should lie in the 1.9 GeV mass region, according to gluon flux tube models [18]. Lattice QCD also predicts the lightest hybrid, an exotic 1^{-+}, at a mass of 1.8 to 1.9 GeV [19]. However, the bag model predicts four nonets, among them an exotic 1^{-+} around or above 1.4 GeV [20,21]. There are so far two candidates for exotic states with quantum numbers 1^{-+}, the $\pi_1(1400)$ and $\pi_1(1600)$, which could be hybrids or four-quark states (see the "Note on Non-$q\bar{q}$ Mesons" in the Meson Listings and in Ref. 17)

15.4. Baryons: *qqq* states

Baryons are fermions with baryon number $\mathcal{B} = 1$, *i.e.*, in the most general case, they are composed of three quarks plus any number of quark - antiquark pairs. So far all established baryons are 3-quark (qqq) configurations (the LHCb collaboration has very recently announced observation of two charmed 'pentaquark' states of minimal quark content $c\bar{c}uud$ at invariant masses close to 4.4 GeV [23]). The color part of their state functions is an SU(3) singlet, a completely antisymmetric state of the three colors. Since the quarks are fermions, the state function must be antisymmetric under interchange of

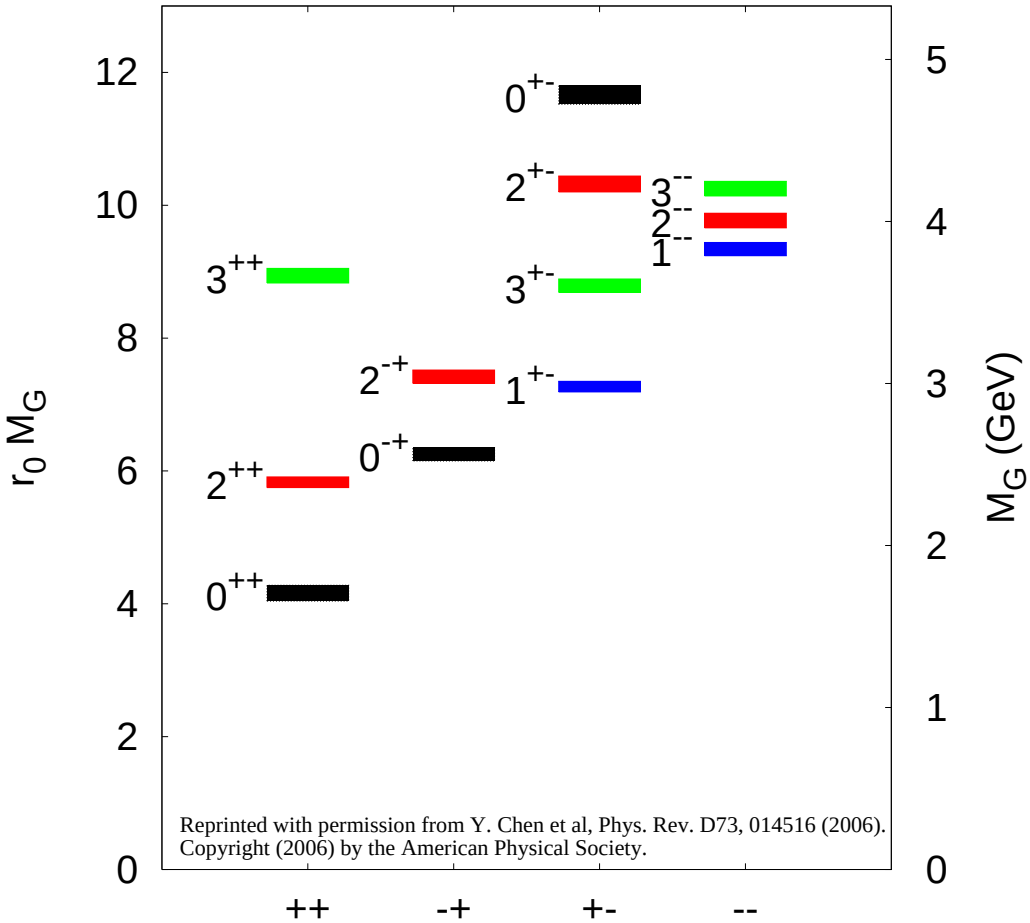

Figure 15.3: Predicted glueball mass spectrum from the lattice in quenched approximation (from Ref. 11)

any two equal-mass quarks (up and down quarks in the limit of isospin symmetry). Thus it can be written as

$$|\, qqq \,\rangle_A = |\, \text{color} \,\rangle_A \times |\, \text{space, spin, flavor} \,\rangle_S \ , \tag{15.21}$$

where the subscripts S and A indicate symmetry or antisymmetry under interchange of any two equal-mass quarks. Note the contrast with the state function for the three nucleons in ^{3}H or ^{3}He:

$$|\, NNN \,\rangle_A = |\, \text{space, spin, isospin} \,\rangle_A \ . \tag{15.22}$$

This difference has major implications for internal structure, magnetic moments, *etc.* (For a nice discussion, see Ref. 24)

The "ordinary" baryons are made up of u, d, and s quarks. The three flavors imply an approximate flavor SU(3), which requires that baryons made of these quarks belong to the multiplets on the right side of

$$\mathbf{3} \otimes \mathbf{3} \otimes \mathbf{3} = \mathbf{10}_S \oplus \mathbf{8}_M \oplus \mathbf{8}_M \oplus \mathbf{1}_A \tag{15.23}$$

(see Sec. 46, on "SU(n) Multiplets and Young Diagrams"). Here the subscripts indicate symmetric, mixed-symmetry, or antisymmetric states under interchange of any two quarks. The **1** is a *uds* state (Λ_1), and the octet contains a similar state (Λ_8). If these have the same spin and parity, they can mix. The mechanism is the same as for the mesons (see above). In the ground state multiplet, the SU(3) flavor singlet Λ_1 is forbidden by Fermi statistics. Section 45, on "SU(3) Isoscalar Factors and Representation Matrices," shows how relative decay rates in, say, $\mathbf{10} \to \mathbf{8} \otimes \mathbf{8}$ decays may be calculated.

The addition of the c quark to the light quarks extends the flavor symmetry to SU(4). However, due to the large mass of the c quark, this symmetry is much more strongly broken than the SU(3) of the three light quarks. Figures 15.4(a) and 15.4(b) show the SU(4) baryon multiplets that have as their bottom levels an SU(3) octet, such as the octet that includes the nucleon, or an SU(3) decuplet, such as the decuplet that includes the $\Delta(1232)$. All particles in a given SU(4) multiplet have the same spin and parity. The charmed baryons are discussed in more detail in the "Note on Charmed Baryons" in the Particle Listings. The same multiplets as shown in 15.4 can be constructed when the c quark is replaced by the b quark, or they can be embedded in a larger SU(5) group that accounts for all baryons that can be constructed from the five quark flavors. The existence of baryons with t-quarks is very unlikely due to the short lifetime of the t-quark. The heavy quark baryons have recently gained a lot of interest. Their relatively narrow widths allow to isolate the states much easier than the light quark baryon resonances which require intricate partial wave analyses. The only problem on the experimental side are the small production cross sections, but the recent measurements at the e^+e^- colliding B factories, at the $p\bar{p}$ Tevatron collider, and at LHCb at CERN have boosted this field. A recent summary is given in Ref. 25. A possible candidate for a doubly charmed baryon had been reported by the SELEX experiment [26,27] but could so far not be confirmed by other experiments, and quark model predictions for baryons with two heavy quarks are given in Ref. 28.

For the "ordinary" baryons (no c or b quark), flavor and spin may be combined in an approximate flavor-spin SU(6), in which the six basic states are $d\uparrow$, $d\downarrow$, $\cdots$, $s\downarrow$ ($\uparrow, \downarrow =$ spin up, down). Then the baryons belong to the multiplets on the right side of

$$\mathbf{6} \otimes \mathbf{6} \otimes \mathbf{6} = \mathbf{56}_S \oplus \mathbf{70}_M \oplus \mathbf{70}_M \oplus \mathbf{20}_A \ . \tag{15.24}$$

These SU(6) multiplets decompose into flavor SU(3) multiplets as follows:

$$\mathbf{56} = {}^4\mathbf{10} \oplus {}^2\mathbf{8} \tag{15.25a}$$

$$\mathbf{70} = {}^2\mathbf{10} \oplus {}^4\mathbf{8} \oplus {}^2\mathbf{8} \oplus {}^2\mathbf{1} \tag{15.25b}$$

$$\mathbf{20} = {}^2\mathbf{8} \oplus {}^4\mathbf{1} \ , \tag{15.25c}$$

where the superscript $(2S+1)$ gives the net spin S of the quarks for each particle in the SU(3) multiplet. The $J^P = 1/2^+$ octet containing the nucleon and the $J^P = 3/2^+$ decuplet containing the $\Delta(1232)$ together make up the "ground-state" 56-plet, in which the orbital angular momenta between the quark pairs are zero (so that the spatial part of the state function is trivially symmetric). The **70** and **20** require some excitation

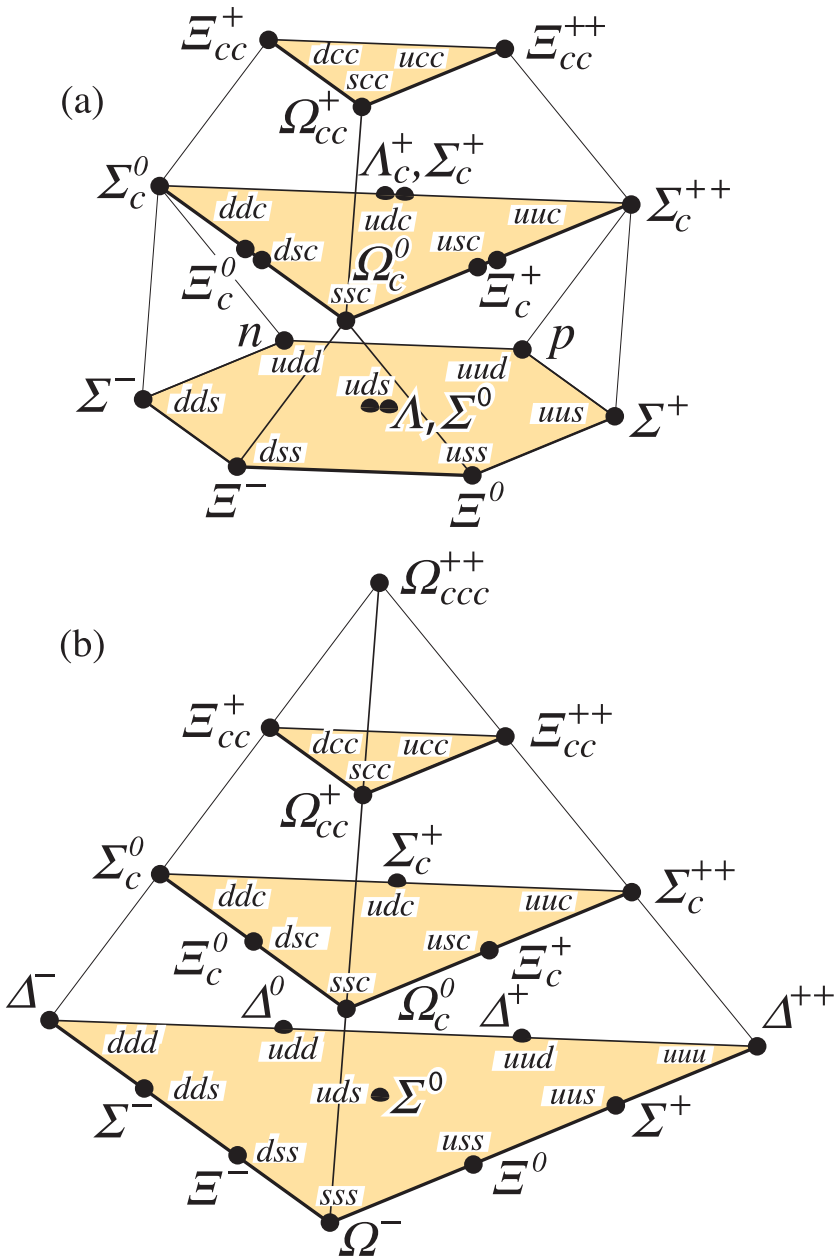

Figure 15.4: SU(4) multiplets of baryons made of u, d, s, and c quarks. (a) The 20-plet with an SU(3) octet. (b) The 20-plet with an SU(3) decuplet.

of the spatial part of the state function in order to make the overall state function symmetric. States with nonzero orbital angular momenta are classified in SU(6)⊗O(3) supermultiplets.

It is useful to classify the baryons into bands that have the same number N of quanta of excitation. Each band consists of a number of supermultiplets, specified by (D, L_N^P), where D is the dimensionality of the SU(6) representation, L is the total quark orbital angular momentum, and P is the total parity. Supermultiplets contained in bands up to

N = 12 are given in Ref. 29. The N = 0 band, which contains the nucleon and $\Delta(1232)$, consists only of the $(56,0_0^+)$ supermultiplet. The N = 1 band consists only of the $(70,1_1^-)$ multiplet and contains the negative-parity baryons with masses below about 1.9 GeV. The N = 2 band contains five supermultiplets: $(56,0_2^+)$, $(70,0_2^+)$, $(56,2_2^+)$, $(70,2_2^+)$, and $(20,1_2^+)$.

Table 15.5: N and Δ states in the N=0,1,2 harmonic oscillator bands. L^P denotes angular momentum and parity, S the three-quark spin and 'sym'=A,S,M the symmetry of the spatial wave function. Only dominant components indicated. Assignments in the N=2 band are partly tentative.

N	sym	L^P	S	$N(I=1/2)$				$\Delta(I=3/2)$			
2	A	1^+	1/2	$1/2^+$	$3/2^+$						
2	M	2^+	3/2	$1/2^+$	$3/2^+$	$5/2^+$	$7/2^+$				
2	M	2^+	1/2		$3/2^+$	$5/2^+$			$3/2^+$	$5/2^+$	
2	M	0^+	3/2		$3/2^+$						
2	M	0^+	1/2	$1/2^+$				$1/2^+$			
				$N(1710)$				$\Delta(1750)$			
2	S	2^+	3/2					$1/2^+$	$3/2^+$	$5/2^+$	$7/2^+$
								$\Delta(1910)$	$\Delta(1920)$	$\Delta(1905)$	$\Delta(1950)$
2	S	2^+	1/2		$3/2^+$	$5/2^+$					
					$N(1720)$	$N(1680)$					
2	S	0^+	3/2						$3/2^+$		
									$\Delta(1600)$		
2	S	0^+	1/2	$1/2^+$							
				$N(1440)$							
1	M	1^-	3/2	$1/2^-$	$3/2^-$	$5/2^-$					
				$N(1650)$	$N(1700)$	$N(1675)$					
1	M	1^-	1/2	$1/2^-$	$3/2^-$			$1/2^-$	$3/2^-$		
				$N(1535)$	$N(1520)$			$\Delta(1620)$	$\Delta(1700)$		
0	S	0^+	3/2						$3/2^+$		
									$\Delta(1232)$		
0	S	0^+	1/2	$1/2^+$							
				$N(938)$							

The wave functions of the non-strange baryons in the harmonic oscillator basis are

Table 15.6: Quark-model assignments for some of the known baryons in terms of a flavor-spin SU(6) basis. Only the dominant representation is listed. Assignments for several states, especially for the $\Lambda(1810)$, $\Lambda(2350)$, $\Xi(1820)$, and $\Xi(2030)$, are merely educated guesses. † recent suggestions for assignments and re-assignments from Ref. 33. For assignments of the charmed baryons, see the "Note on Charmed Baryons" in the Particle Listings.

J^P	$(D, L_N^P)\,S$	Octet members				Singlets
$1/2^+$	$(56,0_0^+)$	$1/2\,N(939)$	$\Lambda(1116)$	$\Sigma(1193)$	$\Xi(1318)$	
$1/2^+$	$(56,0_2^+)$	$1/2\,N(1440)$	$\Lambda(1600)$	$\Sigma(1660)$	$\Xi(1690)^\dagger$	
$1/2^-$	$(70,1_1^-)$	$1/2\,N(1535)$	$\Lambda(1670)$	$\Sigma(1620)$	$\Xi(?)$	$\Lambda(1405)$
				$\Sigma(1560)^\dagger$		
$3/2^-$	$(70,1_1^-)$	$1/2\,N(1520)$	$\Lambda(1690)$	$\Sigma(1670)$	$\Xi(1820)$	$\Lambda(1520)$
$1/2^-$	$(70,1_1^-)$	$3/2\,N(1650)$	$\Lambda(1800)$	$\Sigma(1750)$	$\Xi(?)$	
				$\Sigma(1620)^\dagger$		
$3/2^-$	$(70,1_1^-)$	$3/2\,N(1700)$	$\Lambda(?)$	$\Sigma(1940)^\dagger$	$\Xi(?)$	
$5/2^-$	$(70,1_1^-)$	$3/2\,N(1675)$	$\Lambda(1830)$	$\Sigma(1775)$	$\Xi(1950)^\dagger$	
$1/2^+$	$(70,0_2^+)$	$1/2\,N(1710)$	$\Lambda(1810)$	$\Sigma(1880)$	$\Xi(?)$	$\Lambda(1810)^\dagger$
$3/2^+$	$(56,2_2^+)$	$1/2\,N(1720)$	$\Lambda(1890)$	$\Sigma(?)$	$\Xi(?)$	
$5/2^+$	$(56,2_2^+)$	$1/2\,N(1680)$	$\Lambda(1820)$	$\Sigma(1915)$	$\Xi(2030)$	
$7/2^-$	$(70,3_3^-)$	$1/2\,N(2190)$	$\Lambda(?)$	$\Sigma(?)$	$\Xi(?)$	$\Lambda(2100)$
$9/2^-$	$(70,3_3^-)$	$3/2\,N(2250)$	$\Lambda(?)$	$\Sigma(?)$	$\Xi(?)$	
$9/2^+$	$(56,4_4^+)$	$1/2\,N(2220)$	$\Lambda(2350)$	$\Sigma(?)$	$\Xi(?)$	
		Decuplet members				
$3/2^+$	$(56,0_0^+)$	$3/2\,\Delta(1232)$	$\Sigma(1385)$	$\Xi(1530)$	$\Omega(1672)$	
$3/2^+$	$(56,0_2^+)$	$3/2\,\Delta(1600)$	$\Sigma(1690)^\dagger$	$\Xi(?)$	$\Omega(?)$	
$1/2^-$	$(70,1_1^-)$	$1/2\,\Delta(1620)$	$\Sigma(1750)^\dagger$	$\Xi(?)$	$\Omega(?)$	
$3/2^-$	$(70,1_1^-)$	$1/2\,\Delta(1700)$	$\Sigma(?)$	$\Xi(?)$	$\Omega(?)$	
$5/2^+$	$(56,2_2^+)$	$3/2\,\Delta(1905)$	$\Sigma(?)$	$\Xi(?)$	$\Omega(?)$	
$7/2^+$	$(56,2_2^+)$	$3/2\,\Delta(1950)$	$\Sigma(2030)$	$\Xi(?)$	$\Omega(?)$	
$11/2^+$	$(56,4_4^+)$	$3/2\,\Delta(2420)$	$\Sigma(?)$	$\Xi(?)$	$\Omega(?)$	

often labeled by $|X^{2S+1}L_\pi J^P\rangle$, where S, L, J, P are as above, $X = N$ or Δ, and $\pi = S, M$ or A denotes the symmetry of the spatial wave function. The possible model states for the

bands with N=0,1,2 are given in Table 15.5. The assignment of experimentally observed states is only complete and well established up to the N=1 band. Some more tentative assignments for higher multiplets are suggested in Ref. 30.

In Table 15.6, quark-model assignments are given for many of the established baryons whose SU(6)⊗O(3) compositions are relatively unmixed. One must, however, keep in mind that apart from the mixing of the Λ singlet and octet states, states with same J^P but different L, S combinations can also mix. In the quark model with one-gluon exchange motivated interactions, the size of the mixing is determined by the relative strength of the tensor term with respect to the contact term (see below). The mixing is more important for the decay patterns of the states than for their positions. An example are the lowest lying $(70, 1_1^-)$ states with J^P=1/2$^-$ and 3/2$^-$. The physical states are:

$$|\,N(1535)1/2^-\rangle = \cos(\Theta_S)|N^2P_M1/2^-\rangle - \sin(\Theta_S)|N^4P_M1/2^-\rangle \tag{15.26}$$

$$|\,N(1520)3/2^-\rangle = \cos(\Theta_D)|N^2P_M3/2^-\rangle - \sin(\Theta)_D|N^4P_M3/2^-\rangle \tag{15.27}$$

and the orthogonal combinations for $N(1650)1/2^-$ and $N(1700)3/2^-$. The mixing is large for the J^P=1/2$^-$ states ($\Theta_S \approx$ -32°), but small for the J^P=3/2$^-$ states ($\Theta_D \approx$ +6°) [31,32].

All baryons of the ground state multiplets are known. Many of their properties, in particular their masses, are in good agreement even with the most basic versions of the quark model, including harmonic (or linear) confinement and a spin-spin interaction, which is responsible for the octet - decuplet mass shifts. A consistent description of the ground-state electroweak properties, however, requires refined relativistic constituent quark models.

The situation for the excited states is much less clear. The assignment of some experimentally observed states with strange quarks to model configurations is only tentative and in many cases candidates are completely missing. Recently, Melde, Plessas and Sengl [33] have calculated baryon properties in relativistic constituent quark models, using one-gluon exchange and Goldstone-boson exchange for the modeling of the hyperfine interactions (see Sec. 15.5 on Dynamics). Both types of models give qualitatively comparable results, and underestimate in general experimentally observed decay widths. Nevertheless, in particular on the basis of the observed decay patterns, the authors have assigned some additional states with strangeness to the SU(3) multiplets and suggest re-assignments for a few others. Among the new assignments are states with weak experimental evidence (two or three star ratings) and partly without firm spin/parity assignments, so that further experimental efforts are necessary before final conclusions can be drawn. We have added their suggestions in Table 15.6.

In the non-strange sector there are two main problems which are illustrated in Fig. 15.5, where the experimentally observed excitation spectrum of the nucleon (N and Δ resonances) is compared to the results of a typical quark model calculation [34]. The lowest states from the N=2 band, the $N(1440)1/2^+$, and the $\Delta(1600)3/2^+$, appear lower than the negative parity states from the N=1 band (see Table 15.5) and much lower than predicted by most models. Also negative parity Δ states from the N=3 band ($\Delta(1900)1/2^-$, $\Delta(1940)3/2^-$, and $\Delta(1930)5/2-$) are too low in energy. Part of

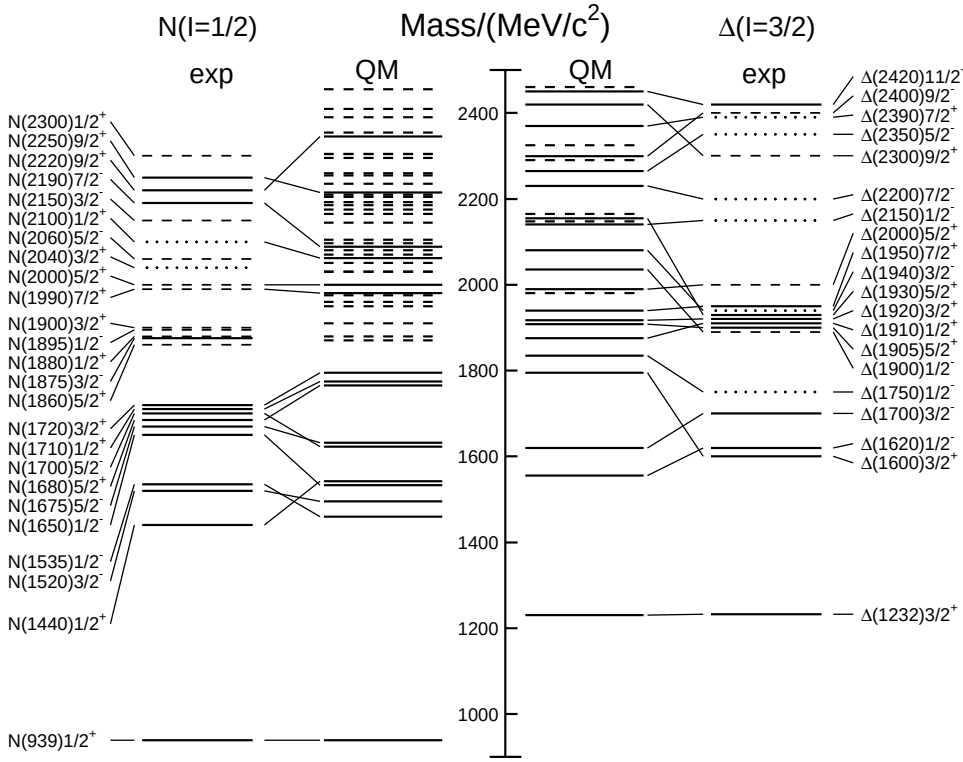

Figure 15.5: Excitation spectrum of the nucleon. Compared are the positions of the excited states identified in experiment, to those predicted by a relativized quark model calculation. Left hand side: isospin $I = 1/2$ N-states, right hand side: isospin $I = 3/2$ Δ-states. Experimental: (columns labeled 'exp'), three- and four-star states are indicated by full lines (two-star dashed lines, one-star dotted lines). At the very left and right of the figure, the spectroscopic notation of these states is given. Quark model [34]: (columns labeled 'QM'), all states for the N=1,2 bands, low-lying states for the N=3,4,5 bands. Full lines: at least tentative assignment to observed states, dashed lines: so far no observed counterparts. Many of the assignments between predicted and observed states are highly tentative.

the problem could be experimental. Among the negative parity Δ states, only the $\Delta(1930)5/2^-$ has three stars and the uncertainty in the position of the $\Delta(1600)3/2^+$ is large (1550 - 1700 MeV).

Furthermore, many more states are predicted than observed. This has been known for a long time as the 'missing resonance' problem [31]. Up to an excitation energy of 2.4 GeV, about 45 N states are predicted, but only 14 are established (four- or three-star; see Note on N and Δ Resonances for the rating of the status of resonances) and 10 are tentative (two- or one-star). Even for the N=2 band, up to now only half of the predicted states have been observed. The most recent partial wave analysis of elastic pion scattering and charge exchange data by Arndt and collaborators [35] has made the situation even worse. They found no evidence for almost half of the states listed in this review (and included in Fig. 15.5). Such analyses are of course biased against resonances

which couple only weakly to the $N\pi$ channel. Quark model predictions for the couplings to other hadronic channels and to photons are given in Ref. 34. A large experimental effort is ongoing at several electron accelerators to study the baryon resonance spectrum with real and virtual photon-induced meson production reactions. This includes the search for as-yet-unobserved states, as well as detailed studies of the properties of the low lying states (decay patterns, electromagnetic couplings, magnetic moments, *etc.*) (see Ref. 36 for recent reviews). This experimental effort has currently entered its final phase with the measurement of single and double polarization observables for many different meson production channels, so that a much better understanding of the experimental spectrum can be expected for the near future.

In quark models, the number of excited states is determined by the effective degrees of freedom, while their ordering and decay properties are related to the residual quark - quark interaction. An overview of quark models for baryons is given in Ref. 32, recent discussions of baryon spectroscopy are given in Refs. 30 and 25. The effective degrees of freedom in the standard nonrelativistic quark model are three equivalent valence quarks with one-gluon exchange-motivated, flavor-independent color-magnetic interactions. The QCD aspect of gluon-gluon interactions is emphasized by the hypercentral quark model [37], [38], which includes in a natural way three-body forces between the quarks. A different class of models uses interactions which give rise to a quark - diquark clustering of the baryons: for a review see Ref. 39. If there is a tightly bound diquark, only two degrees of freedom are available at low energies, and thus *fewer* states are predicted. Furthermore, selection rules in the decay pattern may arise from the quantum numbers of the diquark. *More* states are predicted by collective models of the baryon like the algebraic approach in Ref. 40. In this approach, the quantum numbers of the valence quarks are distributed over a Y-shaped string-like configuration, and additional states arise *e.g.*, from vibrations of the strings. *More* states are also predicted in the framework of flux-tube models, see Ref. 41, which are motivated by lattice QCD. In addition to the quark degrees of freedom, flux-tubes responsible for the confinement of the quarks are considered as degrees of freedom. These models include hybrid baryons containing explicit excitations of the gluon fields. However, since all half integral J^P quantum numbers are possible for ordinary baryons, such 'exotics' will be very hard to identify, and probably always mix with ordinary states. So far, the experimentally observed number of states is still far lower even than predicted by the quark–diquark models.

Recently, the influence of chiral symmetry on the excitation spectrum of the nucleon has been hotly debated from a somewhat new perspective. Chiral symmetry, the fundamental symmetry of QCD, is strongly broken for the low lying states, resulting in large mass differences of parity partners like the J^P=1/2$^+$ $N(938)1/2^+$ ground state and the J^P=1/2$^-$ $N(1535)1/2^-$ excitation. However, at higher excitation energies there is some evidence for parity doublets and even some very tentative suggestions for full chiral multiplets of N^* and Δ resonances. An effective restoration of chiral symmetry at high excitation energies due to a decoupling from the quark condensate of the vacuum has been discussed (see Ref. 42 for recent reviews) as a possible cause. In this case, the mass generating mechanisms for low and high lying states would be essentially different. As a further consequence, the parity doublets would decouple from pions, so that experimental bias would be worse. However, parity doublets might also arise from the spin-orbital

dynamics of the 3-quark system. Presently, the status of data does not allow final conclusions.

The most recent developments on the theory side are the first unquenched lattice calculations for the excitation spectrum discussed in Sec. 15.6. The results are basically consistent with the level counting of SU(6)⊗O(3) in the standard non-relativistic quark model and show no indication for quark-diquark structures or parity doubling. Consequently, there is as yet no indication from lattice that the mis-match between the excitation spectrum predicted by the standard quark model and experimental observations is due to inappropriate degrees of freedom in the quark model.

15.5. Dynamics

Quantum chromodynamics (QCD) is well-established as the theory for the strong interactions. As such, one of the goals of QCD is to predict the spectrum of strongly-interacting particles. To date, the only first-principles calculations of spectroscopy from QCD use lattice methods. These are the subject of Sec. 15.6. These calculations are difficult and unwieldy, and many interesting questions do not have a good lattice-based method of solution. Therefore, it is natural to build models, whose ingredients are abstracted from QCD, or from the low-energy limit of QCD (such as chiral Lagrangians) or from the data itself. The words "quark model" are a shorthand for such phenomenological models. Many specific quark models exist, but most contain a similar basic set of dynamical ingredients. These include:

i) A confining interaction, which is generally spin-independent (*e.g.*, harmonic oscillator or linear confinement);

ii) Different types of spin-dependent interactions:

a) commonly used is a color-magnetic flavor-independent interaction modeled after the effects of gluon exchange in QCD (see *e.g.*, Ref. 43) For example, in the S-wave states, there is a spin-spin hyperfine interaction of the form

$$H_{HF} = -\alpha_S M \sum_{i>j} (\vec{\sigma}\lambda_a)_i (\vec{\sigma}\lambda_a)_j \ , \tag{15.28}$$

where M is a constant with units of energy, λ_a $(a = 1, \cdots, 8,)$ is the set of SU(3) unitary spin matrices, defined in Sec. 45, on "SU(3) Isoscalar Factors and Representation Matrices," and the sum runs over constituent quarks or antiquarks. Spin-orbit interactions, although allowed, seem to be small in general, but a tensor term is responsible for the mixing of states with the same J^P but different L, S combinations.

b) other approaches include flavor-dependent short-range quark forces from instanton effects (see *e.g.*, Ref. 44) This interaction acts only on scalar, isoscalar pairs of quarks in a relative S-wave state:

$$\langle q^2; S, L, T|W|q^2; S, L, T\rangle = -4g\delta_{S,0}\delta_{L,0}\delta_{I,0}\mathcal{W} \tag{15.29}$$

where $\mathcal{W}$ is the radial matrix element of the contact interaction.

c) a rather different and controversially discussed approach is based on flavor-dependent spin-spin forces arising from one-boson exchange. The interaction term is of the form:

$$H_{HF} \propto \sum_{i<j} V(\vec{r}_{ij}) \lambda_i^F \cdot \lambda_j^F \vec{\sigma}_i \cdot \vec{\sigma}_j \tag{15.30}$$

where the λ_i^F are in flavor space (see *e.g.*, Ref. 45).

iii) A strange quark mass somewhat larger than the up and down quark masses, in order to split the SU(3) multiplets;

iv) In the case of spin-spin interactions (iia,c), a flavor-symmetric interaction for mixing $q\overline{q}$ configurations of different flavors (*e.g.*, $u\overline{u} \leftrightarrow d\overline{d} \leftrightarrow s\overline{s}$), in isoscalar channels, so as to reproduce *e.g.*, the η - η' and ω - ϕ mesons.

These ingredients provide the basic mechanisms that determine the hadron spectrum in the standard quark model.

15.6. Lattice Calculations of Hadronic Spectroscopy

Lattice calculations are a major source of information about QCD masses and matrix elements. The necessary theoretical background is given in Sec. 18 of this *Review*. Here we confine ourselves to some general comments and illustrations of lattice calculations for spectroscopy.

In general, the cleanest lattice results come from computations of processes in which there is only one particle in the simulation volume. These quantities include masses of hadrons, simple decay constants, like pseudoscalar meson decay constants, and semileptonic form factors (such as the ones appropriate to $B \to Dl\nu$, $Kl\nu$, $\pi l\nu$). The cleanest predictions for masses are for states which have narrow decay widths and are far below any thresholds to open channels, since the effects of final state interactions are not yet under complete control on the lattice. As a simple corollary, the lightest state in a channel is easier to study than the heavier ones. "Difficult" states for the quark model (such as exotics) are also difficult for the lattice because of the lack of simple operators which couple well to them.

Good-quality modern lattice calculations will present multi-part error budgets with their predictions. A small part of the uncertainty is statistical, from sample size. Typically, the quoted statistical uncertainty includes uncertainty from a fit: it is rare that a simulation computes one global quantity which is the desired observable. Simulations which include virtual quark-antiquark pairs (also known as "dynamical quarks" or "sea quarks") are often done at up and down quark mass values heavier than the experimental ones, and it is then necessary to extrapolate in these quark masses. Simulations can work at the physical values of the heavier quarks' masses. They are always done at nonzero lattice spacing, and so it is necessary to extrapolate to zero lattice spacing. Some theoretical input is needed to do this. Much of the uncertainty in these extrapolations is systematic, from the choice of fitting function. Other systematics include the effect of finite simulation volume, the number of flavors of dynamical quarks actually simulated, and technical issues with how these dynamical quarks are included. The particular choice of a fiducial mass (to normalize other predictions) is not standardized; there are many

possible choices, each with its own set of strengths and weaknesses, and determining it usually requires a second lattice simulation from that used to calculate the quantity under consideration.

A systematic error of major historical interest is the "quenched approximation," in which dynamical quarks are simply left out of the simulation. This was done because the addition of these virtual pairs presented an expensive computational problem. No generally-accepted methodology has ever allowed one to correct for quenching effects, short of redoing all calculations with dynamical quarks. Recent advances in algorithms and computer hardware have rendered it obsolete.

With these brief remarks, we turn to examples. The field of lattice QCD simulations is vast, and so it is not possible to give a comprehensive review of them in a small space. The history of lattice QCD simulations is a story of thirty years of incremental improvements in physical understanding, algorithm development, and ever faster computers, which have combined to bring the field to a present state where it is possible to carry out very high quality calculations. We present a few representative illustrations, to show the current state of the art.

By far, the major part of all lattice spectroscopy is concerned with that of the light hadrons, and so we illustrate results in Fig. 15.6, a comprehensive summary provided by A. Kronfeld [46].

Flavor singlet mesons are at the frontier of lattice QCD calculations, because one must include the effects of "annihilation graphs," for the valence q and $\bar{q}$. Recently, several groups, Refs. 6, 53–56, have reported calculations of the η and η' mesons. The numbers of Ref. 6 are typical, finding masses of 573(6) and 947(142) MeV for the η and η'. The singlet-octet mixing angle (in the conventions of Table 15.2) is $\theta_{lin} = -14.1(2.8)^\circ$.

The spectroscopy of mesons containing heavy quarks has become a truly high-precision endeavor. These simulations use Non-Relativistic QCD (NRQCD) or Heavy Quark Effective Theory (HQET), systematic expansions of the QCD Lagrangian in powers of the heavy quark velocity, or the heavy quark mass. Terms in the Lagrangian have obvious quark model analogs, but are derived directly from QCD. For example, the heavy quark potential is a derived quantity, extracted from simulations. Fig. 15.7 shows the mass spectrum for mesons containing at least one heavy (b or c) quark from Ref. 59 It also contains results from Refs. 61 and 62 The calculations uses a discretization of nonrelativistic QCD for bottom quarks with charm and lighter quarks being handled with an improved relativistic action. Four flavors (u, d, s, c) of dynamical quarks are included.

Fig. 15.8 shows a compilation of recent lattice results for doubly and triply charmed baryons, from Ref. 63.

There are a number of reported states near the charmonium-$D-\bar{D}$ threshold, including the X(3872), $D^*_{s0}(2317)$, $Z_c^\pm(3900)$ and X(4140), whose quark composition is obscure (see the "Note on Non-$q\bar{q}$ mesons in the Meson Listings." The current status of lattice studies of these states is reviewed in Ref. 69.

Recall that lattice calculations take operators which are interpolating fields with quantum numbers appropriate to the desired states, compute correlation functions of these operators, and fit the correlation functions to functional forms parametrized by a set of masses and matrix elements. As we move away from hadrons which can be

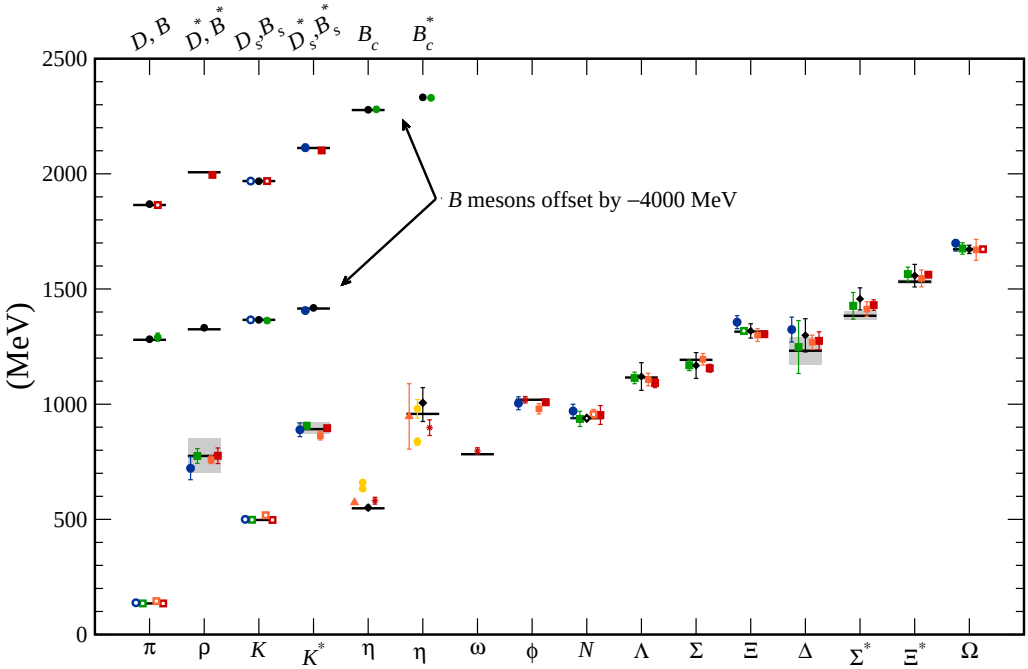

Figure 15.6: Hadron spectrum from lattice QCD. Comprehensive results for mesons and baryons are from MILC [47,48], PACS-CS [49], BMW [50], QCDSF [51], and ETM [68]. Results for η and η' are from RBC & UKQCD [6], Hadron Spectrum [54](also the only ω mass), UKQCD [53], and Michael, Ottnad, and Urbach [55]. Results for heavy-light hadrons from Fermilab-MILC [57], HPQCD [58,59], and Mohler and Woloshyn [60]. Circles, squares, diamonds, and triangles stand for staggered, Wilson, twisted-mass Wilson, and chiral sea quarks, respectively. Asterisks represent anisotropic lattices. Open symbols denote the masses used to fix parameters. Filled symbols (and asterisks) denote results. Red, orange, yellow, green, and blue stand for increasing numbers of ensembles (i.e., lattice spacing and sea quark mass). Black symbols stand for results with 2+1+1 flavors of sea quarks. Horizontal bars (gray boxes) denote experimentally measured masses (widths). b-flavored meson masses are offset by -4000 MeV.

created by the simplest quark model operators (appropriate to the lightest meson and baryon multiplets) we encounter a host of new problems: either no good interpolating fields, or too many possible interpolating fields, and many states with the same quantum numbers. Techniques for dealing with these interrelated problems vary from collaboration to collaboration, but all share common features: typically, correlation functions from many different interpolating fields are used, and the signal is extracted in what amounts to a variational calculation using the chosen operator basis. In addition to mass spectra, wave function information can be garnered from the form of the best variational wave function. Of course, the same problems which are present in the spectroscopy of the lightest hadrons (the need to extrapolate to infinite volume, physical values of the light quark masses, and zero lattice spacing) are also present. We briefly touch on three different kinds of hadrons: excited states of mesons (including hybrids), excited states of

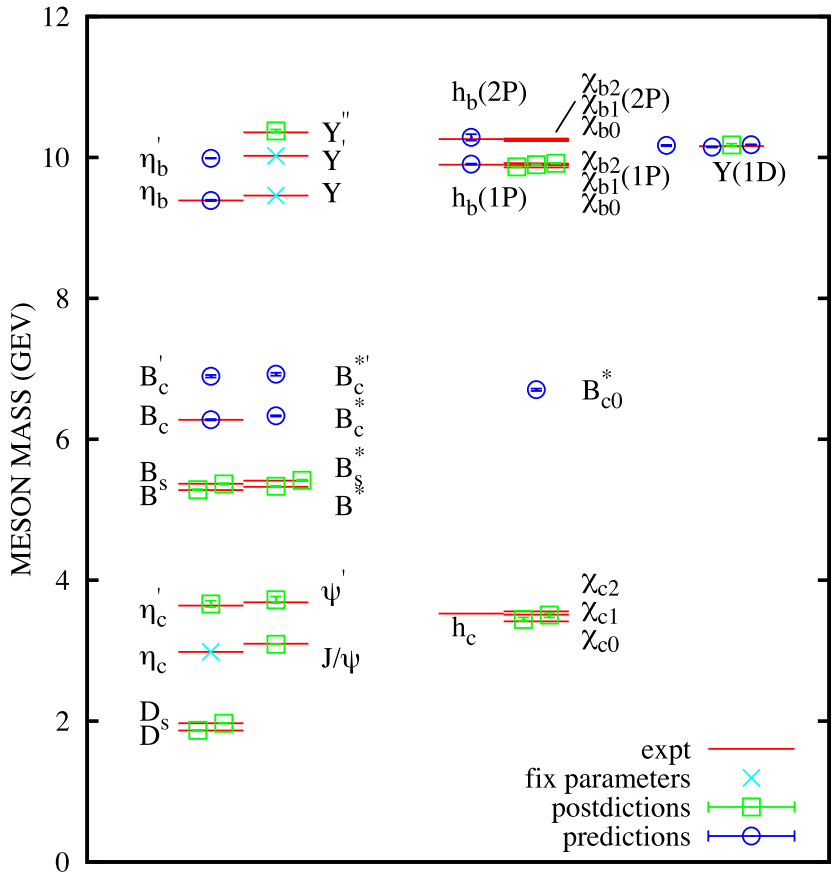

Figure 15.7: Spectroscopy for mesonic systems containing one or more heavy quarks (adapted from Ref. 59) Particles whose masses are used to fix lattice parameters are shown with crosses; the authors distinguish between "predictions" and "postdictions" of their calculation. Lines represent experiment.

baryons, and glueballs. The quality of the data is not as good as for the ground states, and so the results continue to evolve.

Modern calculations use a large bases of trial states, which allow them to probe many quantum number channels simultaneously. This is vital for studying "difficult sectors" of QCD, such as the isoscalar mesons. A recent example of meson spectroscopy where this is done, by Ref. 56, is shown in Fig. 15.9. The quark masses are still heavier than their physical values, so the pion is at 391 MeV. The authors can assign a relative composition of nonstrange and strange quark content to their states, observing, for example, a nonstrange ω and a strange ϕ. Some states also have a substantial component of gluonic excitation. Note especially the three exotic channels $J^{PC} = 1^{-+}$, 0^{+-}, and 2^{+-}, with states around 2 GeV. These calculations will continue to improve as the quark masses are carried lower.

The interesting physics questions of excited baryon spectroscopy to be addressed are precisely those enumerated in the last section. An example of a recent calculation, due to Ref. 70 is shown in Fig. 15.10. Notice that the pion is not yet at its physical value.

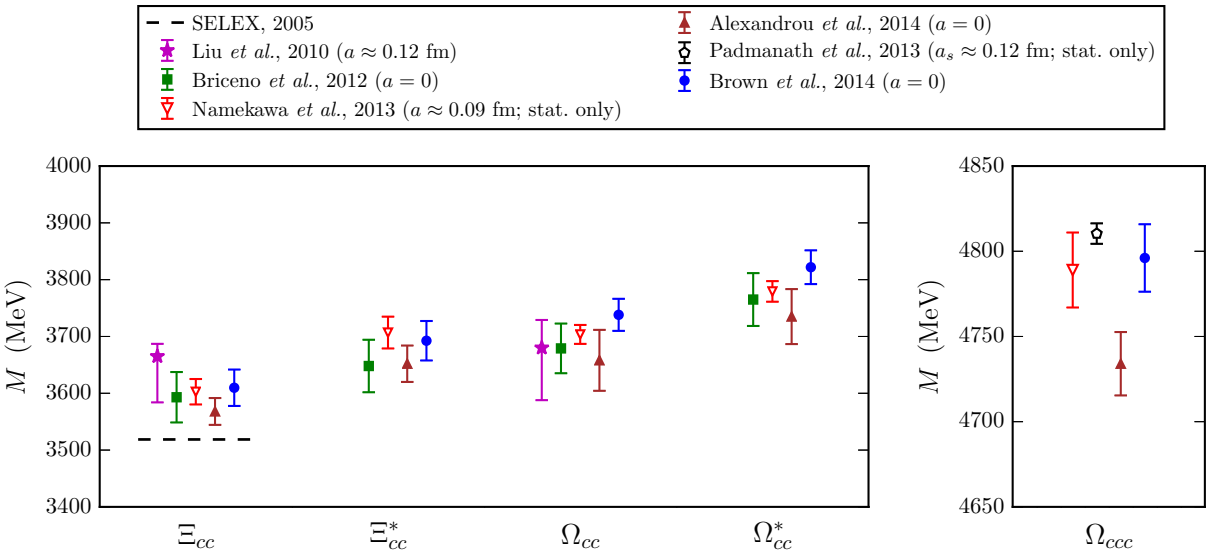

Figure 15.8: Comparison of lattice QCD results for the doubly and triply charmed baryon masses. Labels are Liu, *et al.*, [64]; Briceno, *et al.*, [65]; Namekawa, *et al.*, [66]; Padmanath, *et al.*, [67]; Alexandrou, *et al.*, [68]; and Brown, *et al.*, citequarkmod:Brown:2014ena. Only calculations with dynamical light quarks are included; for the doubly charmed baryons, only calculations were performed at or extrapolated to the physical pion mass are shown. Results without estimates of systematic uncertainties are labeled "stat. only". The lattice spacing values used in the calculations are also given; $a = 0$ indicates that the results have been extrapolated to the continuum limit. In the plot of the doubly charmed baryons, the unconfirmed experimental result for the Ξ_{cc}^{+} mass from SELEX [26,27] is shown with a dashed line.

The lightest positive parity state is the nucleon, and the Roper resonance has not yet appeared as a light state.

In Fig. 15.3 we showed a figure from Ref. 11 presenting a lattice prediction for the glueball mass spectrum in quenched approximation. A true QCD prediction of the glueball spectrum requires dynamical light quarks and (because glueball operators are intrinsically noisy) high statistics. Only recently have the first useful such calculations appeared. Fig. 15.11 shows results from Ref. 71, done with dynamical u, d and s quarks at two lattice spacings, 0.123 and 0.092 fm, along with comparisons to the quenched lattice calculation of Ref. 10 and to experimental isosinglet mesons. The dynamical simulation is, of course, not the last word on this subject, but it shows that the effects of quenching seem to be small.

Several other features of hadronic spectroscopy are also being studied on the lattice.

Electromagnetic mass splittings (such as the neutron - proton mass difference) are interesting but difficult. These calculations are important for determining the values of the quark masses (for a discussion see the review in the PDG). Knowing that the neutron is heavier than the proton tells us that these splittings have a complicated origin. One part of the shift is because the up and down quarks have slightly different masses. The

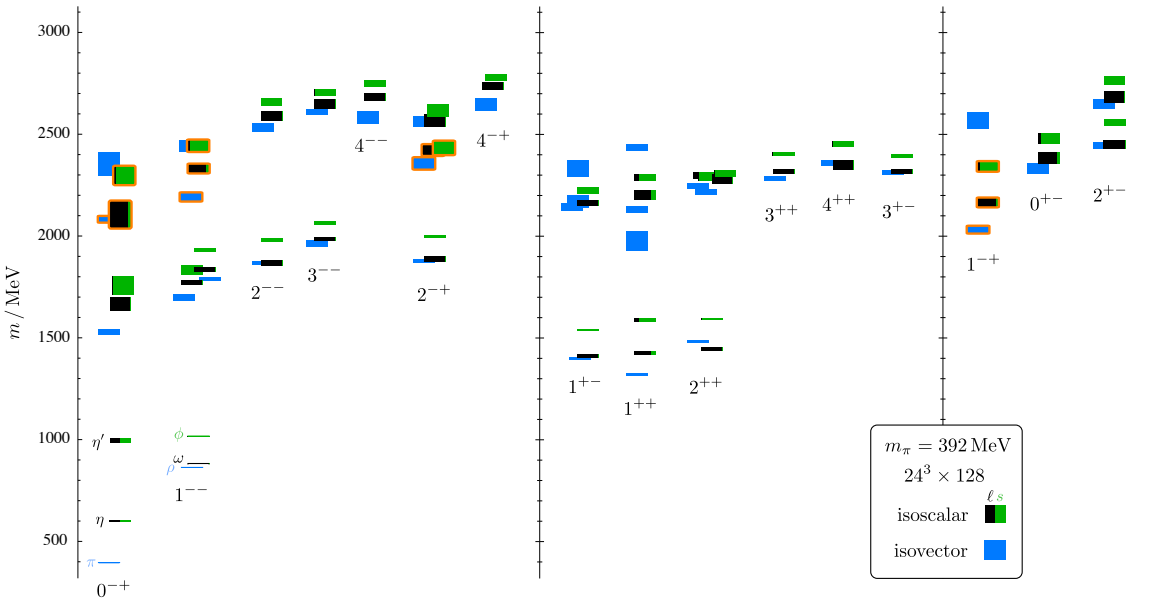

Figure 15.9: Isoscalar (green and black) and isovector (blue) spectrum from Ref. 56. States are labeled J^{PC}. The quark mass is heavier than its physical value; $m_\pi = 391$ MeV. The vertical height of each box indicates the statistical uncertainty in the mass. Black and green indicate relative nonstrange and strange composition. Orange outlines show states with a large chromomagnetic component to their wave function, which the authors of Ref. 56 argue are hybrid states. Note the exotic states in the three rightmost columns.

second is that the quarks have (different) charges. In pre-lattice days, phenomenologists would combine Coulomb forces and spin-dependent electromagnetic hyperfine interactions to model their charge effects. These days, in order to compute hadronic mass differences on the lattice, electromagnetic interactions must be included in the simulations. This creates a host of technical issues. An important one is that electromagnetic interactions are long range, but lattice simulations are done in finite volumes. A recent calculation, Ref. 72, has presented the first results for electromagnetic mass splittings in the baryon octet. The situation is summarized in the review Ref. 73.

Most hadrons are resonances, and their widths are the last target of lattice simulations we will mention. The actual calculation is of the combined mass of two (or more) hadrons in a box of finite size. The combined mass is shifted from being the sum of the individual masses because the finite box forces the hadrons to interact with each other. The volume-dependent mass shift yields the phase shift for the continuum scattering amplitude, which in turn can be used to extract the resonance mass and width, with some degree of modeling. So far only two-body resonances, the rho meson and a few others, have been well studied. This is an active research topic. A recent review, Ref. 74, summarizes the situation, and an example of a calculation of the rho meson's decay width is Ref. 75.

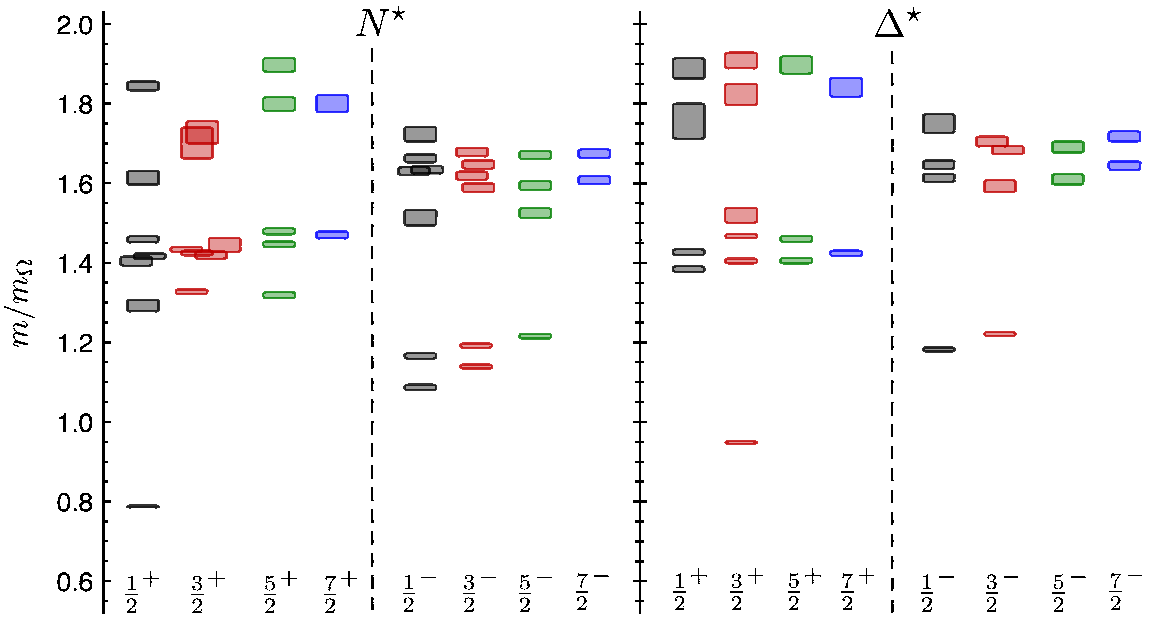

Figure 15.10: Spin-identified spectrum of nucleons and deltas, from lattices where $m_\pi = 396$ MeV, in units of the calculated Ω mass, from Ref. 70. The colors just correspond to the different J assignments: grey for $J = 1/2$, red for $J = 3/2$, green for $5/2$, blue for $J = 7/2$.

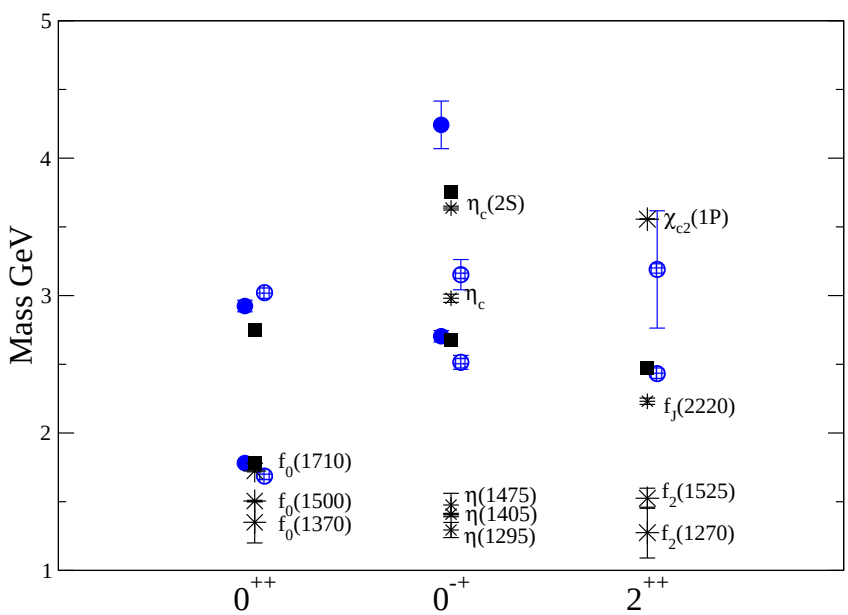

Figure 15.11: Lattice QCD predictions for glueball masses. The open and closed circles are the larger and smaller lattice spacing data of the full QCD calculation of glueball masses of Ref. 71. Squares are the quenched data for glueball masses of Ref. 10. The bursts labeled by particle names are experimental states with the appropriate quantum numbers.

References:

1. J. Schwinger, Phys. Rev. **135**, B116 (1964).
2. A. Bramon *et al.*, Phys. Lett. **B403**, 339 (1997).
3. A. Aloisio *et al.*, Phys. Lett. **B541**, 45 (2002).
4. C. Amsler *et al.*, Phys. Lett. **B294**, 451 (1992).
5. C. Amsler, Rev. Mod. Phys. **70**, 1293 (1998).
6. N.H. Christ *et al.*, Phys. Rev. Lett. **105**, 241601 (2010).
7. T. Feldmann, Int. J. Mod. Phys. **A915**, 159 (2000).
8. C. Amsler and F.E. Close, Phys. Rev. **D53**, 295 (1996).
9. R.L. Jaffe, Phys. Rev. **D15**, 267 (1977);
   R.L. Jaffe, Phys. Rev. **D15**, 281 (1977).
10. C. Morningstar and M. Peardon, Phys. Rev. **D60**, 034509 (1999).
11. Y. Chen *et al.*, Phys. Rev. **D73**, 014516 (2006).
12. W.J. Lee and D. Weingarten, Phys. Rev. **D61**, 014015 (2000).
13. G.S. Bali *et al.*, Phys. Lett. **B309**, 378 (1993).
14. C. Michael, *AIP Conf. Proc.* **432**, 657 (1998).
15. F.E. Close and A. Kirk, Eur. Phys. J. **C21**, 531 (2001).
16. W. Ochs, J. Phys. **G40**, 043001 (2013).
17. C. Amsler and N.A. Törnqvist, Phys. Reports **389**, 61 (2004).
18. N. Isgur and J. Paton, Phys. Rev. **D31**, 2910 (1985).
19. P. Lacock *et al.*, Phys. Lett. **B401**, 308 (1997);
    C. Bernard *et al.*, Phys. Rev. **D56**, 7039 (1997);
    C. Bernard *et al.*, Phys. Rev. **D68**, 074505 (2003).
20. M. Chanowitz and S. Sharpe, Nucl. Phys. **B222**, 211 (1983).
21. T. Barnes *et al.*, Nucl. Phys. **B224**, 241 (1983).
22. W.-M Yao *et al.*, J. Phys. **G33**, 1 (2006).
23. R. Aaij *et al.*, Phys. Rev. Lett. **115**, 072001 (2015).
24. F.E. Close, in *Quarks and Nuclear Forces* (Springer-Verlag, 1982), p. 56.
25. V. Crede and W. Roberts, Rept. on Prog. in Phys. **76**, 076301 (2013).
26. M. Mattson *et al.*, Phys. Rev. Lett. **89**, 112001 (2002).
27. A. Ocherashvili *et al.*, Phys. Lett. **B628**, 18 (2005).
28. M. Karliner and J.L. Rosner, Phys. Rev. **D90**, 094007 (2014).
29. R.H. Dalitz and L.J. Reinders, in "Hadron Structure as Known from Electromagnetic and Strong Interactions," *Proceedings of the Hadron '77 Conference* (Veda, 1979), p. 11.
30. E. Klempt and J.M. Richard, Rev. Mod. Phys. **82**, 1095 (2010).
31. N. Isgur and G. Karl, Phys. Rev. **D18**, 4187 (1978); *ibid.*, **D19**, 2653 (1979); *ibid.*, **D20**, 1191 (1979).
32. S. Capstick and W. Roberts, Prog. in Part. Nucl. Phys. **45**, 241 (2000).
33. T. Melde, W. Plessas, and B. Sengl, Phys. Rev. **D77**, 114002 (2008).
34. S. Capstick and W. Roberts, Phys. Rev. **D49**, 4570 (1994); *ibid.*, **D57**, 4301 (1998); *ibid.*, **D58**, 074011 (1998);
    S. Capstick, Phys. Rev. **D46**, 2864 (1992).
35. R.A. Arndt *et al.*, Phys. Rev. **C74**, 045205 (2006).

36. B. Krusche and S. Schadmand, Prog. in Part. Nucl. Phys. **51**, 399 (2003);
V.D. Burkert and T.-S.H. Lee, Int. J. Mod. Phys. **E13**, 1035 (2004);
see also A.J.G. Hey and R.L. Kelly, Phys. Reports **96**, 71 (1983).
37. M. Ferraris *et al.*, Phys. Lett. **B364**, 231 (1995).
38. M.M. Giannini and E. Santopinto, Chin. J. Phys. **53**, 020301-1 (2015).
39. M. Anselmino *et al.*, Rev. Mod. Phys. **65**, 1199 (1993).
40. R. Bijker *et al.*, Ann. Phys. **236**, 69 (1994).
41. N. Isgur and J. Paton, Phys. Rev. **D31**, 2910 (1985);
S. Capstick and P.R. Page, Phys. Rev. **C66**, 065204 (2002).
42. R.L. Jaffe, D. Pirjol, and A. Scardicchio, Phys. Rev. **435**, 157 (2006);
L. Ya. Glozman, Phys. Rev. **444**, 1 (2007).
43. A. De Rujula *et al.*, Phys. Rev. **D12**, 147 (1975).
44. W.H. Blask *et al.*, Z. Phys. **A337**, 327 (1990);
U. Löring *et al.*, Eur. Phys. J. **A10**, 309 (2001);
U. Löring *et al.*, Eur. Phys. J. **A10**, 395 (2001); *ibid.*, **A10**, 447 (2001).
45. L.Y. Glozman and D.O. Riska, Phys. Rev. **268**, 263 (1996);
L.Y. Glozman *et al.*, Phys. Rev. **D58**, 094030 (1998);
W. Plessas, Int. J. Mod. Phys. **A30**, 1530013 (2015).
46. A. Kronfeld, private comunication. See also Ann. Rev. Nucl. and Part. Sci. **62**, 265 (2012) for an earlier version of this figure.
47. C. Aubin *et al.*, Phys. Rev. **D70**, 094505 (2004) [`hep-lat/0402030`].
48. A. Bazavov *et al.*, Rev. Mod. Phys. **82**, 1349 (2010) [`arXiv:0903.3598`].
49. S. Aoki *et al.* [PACS-CS Collab.], Phys. Rev. **D79**, 034503 (2009) [`arXiv:0807.1661`].
50. S. Durr *et al.*, Science **322**, 1224 (2008) [`arXiv:0906.3599`].
51. W. Bietenholz *et al.*, Phys. Rev. **D84**, 054509 (2011) [`arXiv:1102.5300`].
52. C. Alexandrou *et al.*, Phys. Rev. **D90**, 074501 (2014) [`arXiv:1406.4310`].
53. E.B. Gregory *et al.* [UKQCD Collab.], Phys. Rev. **D86**, 014504 (2012) [`arXiv:1112.4384`].
54. J.J. Dudek *et al.*, Phys. Rev. **D83**, 111502 (2011) [`arXiv:1102.4299`].
55. C. Michael *et al.* [ETM Collab.], Phys. Rev. Lett. **111**, 181602 (2013) [`arXiv:1310.1207`].
56. J.J. Dudek *et al.* [Hadron Spectrum Collab.], Phys. Rev. **D88**, 094505 (2013) [`arXiv:1309.2608`].
57. C. Bernard *et al.* [Fermilab Lattice and MILC Collab.], Phys. Rev. **D83**, 034503 (2011) [`arXiv:1003.1937`].
58. E.B. Gregory *et al.*, Phys. Rev. **D83**, 014506 (2011) [`arXiv:1010.3848`].
59. R.J. Dowdall *et al.*, Phys. Rev. **D86**, 094510 (2012) [`arXiv:1207.5149`].
60. D. Mohler and R. M. Woloshyn, Phys. Rev. **D84**, 054505 (2011) [`arXiv:1103.5506`].
61. J.O. Daldrop *et al.* [HPQCD Collab.], Phys. Rev. Lett. **108**, 102003 (2012).
62. G.C. Donald *et al.*, Phys. Rev. **D86**, 094501 (2012).
63. Z.S. Brown *et al.*, Phys. Rev. **D90**, 094507 (2014).
64. L. Liu *et al.*, Phys. Rev. **D81**, 094505 (2010).
65. R.A. Briceno, H.-W. Lin, and D.R. Bolton, Phys. Rev. **D86**, 094504 (2012).
66. Y. Namekawa *et al.* [PACS-CS Collab.], Phys. Rev. **D87**, 094512 (2013).

67. M. Padmanath *et al.*, Phys. Rev. **D90**, 074504 (2014).
68. C. Alexandrou *et al.*, Phys. Rev. **D90**, 074501 (2014).
69. S. Prelovsek, PoS LATTICE **2014**, 015 (2014) [arXiv:1411.0405].
70. R.G. Edwards *et al.*, Phys. Rev. **D84**, 074508 (2011) [arXiv:1104.5152].
71. C.M. Richards *et al.*, [UKQCD Collab.], Phys. Rev. **D82**, 034501 (2010).
72. S. Borsanyi *et al.*, Science **347**, 1452 (2015) [arXiv:1406.4088].
73. A. Portelli, PoS LATTICE **2014**, 013 (2015) [arXiv:1505.07057].
74. M. Döring, PoS LATTICE **2013**, 006 (2014)..
75. J.J. Dudek *et al.* [Hadron Spectrum Collab.], Phys. Rev. **D87**, 034505 (2013) [Phys. Rev. **D90**, 099902 (2014)] [arXiv:1212.0830].